A computer program for non-LTE modelling of stellar atmospheres

Description and tests.

A. V. Dodin
Sternberg Astronomical Institute
Moscow State University

e-mail: dodin_nv@mail.ru

Moscow
2014

Contents

I

Description of the code

This section contains a description of the code that was used for a non-LTE modelling of stellar atmosphere, irradiated by an external radiation in the context of matter accretion by young stars. The code is a revised and expanded code of well known program DETAIL (Butler, Giddings, 1985), which calculates non-LTE populations of atomic levels of a few user-defined elements at a fixed atmospheric structure. The program, described here, allows to solve the non-LTE problem self-consistently, i.e. the atmospheric structure and the non-LTE-populations are calculated simultaneously.

I.1. The basic system of equations

A structure of homogeneous plane-parallel atmosphere can be calculated by a solution of the basic equations, described below.

Equation of hydrostatic equilibrium:

$$\frac{dP_{tot}}{dz} = -g\rho, \text{ with the boundary condition: } P_{tot}(z_0) = P_0, \tag{I.1.1}$$

where z – height in the atmosphere, g – gravity, ρ – density, P_{tot} – total pressure:

$$P_{tot} = (N_e + N_a)kT + P_{rad}, \tag{I.1.2}$$

N_e – electron number density, N_a – number density of atoms and ions in all excitation states. The latter quantity is related to the density as: $\rho = \mu m_a N_a$, where μ – the mean molecular weight, in case of solar elemental abundances $\mu \approx 1.26$, m_a – the atomic mass unit.

In order to calculate N_e and level populations $N_l^{t,i}$ in case of LTE, the systen of Saha and Boltzmann equations for each t-th elements should be solved:

$$\frac{N_e N^{t,i+1}}{N^{t,i}} = \frac{2Q^{t,i+1}}{Q^{t,i}} \left(\frac{2\pi m_e kT}{h^2}\right)^{3/2} e^{-\frac{\chi^{t,i+1}}{kT}}, \quad Q^{t,i} = \sum g_l^{t,i} e^{-\frac{E_l^{t,i}}{kT}}, \quad \frac{N_l^{t,i}}{N^{t,i}} = \frac{g_l^{t,i}}{Q^{t,i}} e^{-\frac{E_l^{t,i}}{kT}}. \tag{I.1.3}$$

and in non-LTE-case, the equations of statistical equilibrium should be solved:

$$N_k^t \sum_u R_{ku}^t = \sum_u N_u^t R_{uk}^t, \quad k = 1 : K^t, \quad u = 1 : K^t, \tag{I.1.4}$$

Here N_k^t are the renumbered populations $N_l^{t,i}$, K^t is a full number of levels in an atom and its ions, which are considered in non-LTE. R_{**}^* – transition rates, which depend on

N_e, T, J_ν and cross-sections of atomic processes for each specific transition. Both equations (ref BEq.SB, ref BEq.SE) should be supplemented by conditions of the normalization and the charge conservation:

$$\sum_i \sum_l N_l^{t,i} = N_a^t \tag{I.1.5}$$

$$\sum_{t,i,l} Z^{t,i} N_l^{t,i} = N_e, \tag{I.1.6}$$

where $N_a^t = \xi_t N_a$ is the total numder density of an element with an abundance ξ_t, $Z^{t,i}$ is a charge of an ion.

The gas in the stellar atmosphere exchanges an energy with the radiation field and, in the stationary situation, the heating and cooling must be balanced, that is expressed by the equation of radiative equilibrium:

$$\int_0^\infty \chi_\nu^a J_\nu d\nu = \int_0^\infty j_\nu d\nu. \tag{I.1.7}$$

In absence of energy sources in the atmosphere, in stationary case, the total energy flux is constant throughout the plane atmosphere and is determined only by an effective temperature of the star T_{eff}.

$$\int_0^\infty H_\nu d\nu + H_{conv} = \frac{\sigma T_{eff}^4}{4\pi}, \tag{I.1.8}$$

H_{conv} is convective flux.

To determine moments of the radiation field:

$$J_\nu = \frac{1}{2}\int_{-1}^{1} I_\nu(\mu) d\mu,$$

$$H_\nu = \frac{1}{2}\int_{-1}^{1} I_\nu(\mu)\mu d\mu,$$

the radiative transfer equation should be solved:

$$\mu \frac{dI_\nu(\mu)}{dz} = -(\chi_\nu^a + \chi_\nu^s) I_\nu(\mu) + j_\nu + \chi_\nu^s J_\nu, \tag{I.1.9}$$

The coefficients of a true absorption χ_ν^a, a scattering χ_ν^s, and an emission j_ν can be derived from cross-sections of elementary processes of absorption/scattering and the level populations $N_l^{t,i}$.

The programm DETAIL solves the equations (I.1.3) at a fixed value of N_e and N_a for all elements, the equations (I.1.4) are solved only for a few elements, which are defined by user, who must define for them all the necessary atomic data. DETAIL's subroutines allow to calculate values χ_ν^a, χ_ν^s, j_ν and to solve the radiative transfer equation (I.1.9) by Feautrier's method. The equations (I.1.4) and (I.1.9) are solved in DETAIL self-consistently by using an accelerated Λ-iteration method. In the next section we will consider a structure of a computer program, which allows to solve all equations self-consistently.

I.2. A general structure of the code

1. Reading an input data (Atomic data, initial model, technical parameters).

2. Integration of the hydrostatic equilibrium equation (I.1.1). If we redefine the coordinates z by $m : dm = -\rho dz$, then the hydrostatic equilibrium equation has a solution:

$$P_{tot} = gm + P_0, \tag{I.2.1}$$

   At the present time, the equations (I.1.1-I.1.9) are solved on a fixed grid m with nodes m_d thus during the modelling the total pressure $P_{tot}(m_d) = const$ in each particular node of the grid due to the solution (I.2.1). In order to obtain a solution on a fixed grid of Rosseland optical depth τ^{std}_{Ross}, the model of the atmosphere, including the grid m, should be interpolated (or extrapolated) from the grid τ_{Ross}, which can be calculated for the present set of m_d, to the grid τ^{std}_{Ross}, then the system of the equation (I.1.1-I.1.9) should be solved again on the new grid m.

3. The main iteration loop:

   3.1. Calculating some line profiles by an interpolation from tables. (DETAIL: utable.f90, with minor changes)

   3.2. Solving the Saha and Boltzmann equations at constant gas pressure and temperature. Re-calculating the gas density (significantly modified DETAIL's subroutine: sumup.f90).

   3.3. Calculating χ^a_ν, χ^s_ν, j_ν for elements, treated in LTE (DETAIL: opac.f90, with minor changes).

   3.4. Calculating collisional transition rates. (DETAIL: collis.f90)

   3.5. Getting a self-consistent solution of the radiative transfer equation and the statistical equilibrium equations by using the accelerated Λ-iteration technique (revised DETAIL's subroutines: code.f90: alinvel.f90: formal.f90).

   3.6. Calculating the radiation pressure P_{rad} and re-calculating the gas pressure $P_{gas} = P_{tot} - P_{rad}$.

   3.7. Calculating the convective flux H_{conv} (using mixing length theory, adopted from the TLUSTY code).

   3.8. The temperature correction.

   3.9. The correction of N_a, N_e, in order to keep a constant pressure when the temperature changes.

   The end of the main iteration loop. Iterations are performed until the balance between heating and cooling (I.1.7) is reached and the condition of constant energy flux (I.1.8) is reached.

I.3. Solving the Saha and Boltzmann equations

Let's transform the equations (I.1.3) into a form, which will be used to get a numerical solution for them, omitting the index t for brevity:

$$N^i_l = SB_i N^{i+1}_1, \quad SB_i = CS \frac{g^i_l}{g^{i+1}_1} e^{\frac{I^i_l}{kT}}, \quad CS = \frac{N_e}{2}\left(\frac{h^2}{2\pi m_e kT}\right)^{3/2}, \tag{I.3.1}$$

where I_l^i is an ionization potential of the level l in i-th ion. The ground state of each ion has $l = 1$, and the last considered ion has only the ground state, which can be designated as N_1^K. All N_l^i can be expressed through N_1^K and substituted in the normalization condition (I.1.5). After that N_1^K can be found. The rest N_l^i can be calculated directly from the recurrence relation (I.3.1). Such algorithm leads to overflow problems in case of ions with high ionisation potentials, because an arising sums of products of SB_i can exceed 10^{308} (max double). Hence the programm determines the highest ionization stage, for which SB_i does not exceed e^{100}, and the equations (I.3.1) are considered upto this ion, which will be labeled as K. Level populations of more higher ions are equated to a small number, because in LTE conditions the ions with $I_l^i > 100kT$ have to be in a negligible concentration. However in non-LTE case, an ionizing external radiation can produce a "hot" ions in a "cold" gas, accordingly in case of non-LTE-atoms the values of SB_i are artificially limited by $e^{200} \approx 10^{87}$. It means that the results will be wrong for departures from LTE about 80 orders of magnitude, therefore, we impose a constraint that the departures from LTE cannot exceed 80 orders of magnitude. It turned out that it is sufficient for our calculations. Any significant level populations of the "hot" ions do not deviate from LTE by more than 50 orders of magnitude, in the case of simulation of accretion spots in T Tauri stars.

Our solution of the system of the basic equations (I.1.1-I.1.9) assumes that the Saha and Boltzmann equations have to be solved at fixed values of T, P_{gas}. It means that the solution of (I.3.1) has to be found at fixed $N_{tot} = N_a + N_e$, but not at fixed N_a and N_e, as it is described before. It can be achieved by applying the following iterative procedure. The equations (I.1.5) are solved at initial values of N_a^0 and N_e^0, which can be taken from the previous main iteration or the initial model. After that, a new value of N_e is calculated as $N_e^{new} = \sum_{t,i,l} b_l^{t,i} Z^{t,i} N_l^{t,i}$, where the sum is taken over all levels of all ions, $N_l^{t,i}$ are the LTE populations, and departures from LTE are teken into account by b-In the next step the value $0.5(N_e^0 + N_e^{new})$ is taken as the new value of N_e^0, and N_a^0 is re-calculated as $N_{tot} - N_e^0$. The iteratins are stopped when the relative variation of N_e between two successive iterations became less than 10^{-3}. This typically requires less than 10 iterations, in most cases the initial guess is close enough to the solution and the convergence is achieved in 2 – 3 iteration. If the solution has not been achieved in 1000 iterations, then the program terminates with a corresponding message.

To reduce the computing time, LTE-ions with the relative abundance of a ground state $N_1^{t,i}/N_a < 10^{-10}$ are ignored in a computation of line opacity (i.e. in opacity sampling).

I.4. Solving the radiative transfer equation

A formal solution of the radiative transfer equation (I.1.9) is obtained by Feautrier's method for three directions, which are defined by the cosines μ_i. The values of μ_i and corresponding integration weights w_i are chosen by an 3-point Gaussian quadrature rule:

$$\mu_1 = 0.8872983346, \;\; \mu_2 = 0.5, \;\; \mu_3 = 0.1127016654;$$

$$w_1 = d\mu_1 = 0.277777777778, \;\; w_2 = d\mu_2 = 0.444444444444, \;\; w_3 = d\mu_3 = 0.277777777778.$$

The description of Feautrier's method can be found in Mihalas's book (1978). Here we consider only the questions, related with changes we have made in subroutine formal.f90 of the original DETAIL code.

The radiative transfer equation are solved not for the intensity $I(\mu)$ in the nodes in $\pm\mu_i$, but for a combination:

$$V_i = \frac{I(\mu_i) + I(-\mu_i)}{2}. \tag{I.4.1}$$

The equation (I.1.9) in new variable takes the form:

$$\mu_i^2 \frac{d^2 V_i}{d\tau^2} = V_i - (1-\epsilon)S - \epsilon \sum V_i w_i, \tag{I.4.2}$$

with an upper boundary condition:

$$\mu_i \frac{dV_i}{d\tau} = V_i - I_{ei} \text{ at } \tau = 0, \tag{I.4.3}$$

and with a lower boundary condition:

$$\mu_i \frac{dV_i}{d\tau} + V_i = S + \mu_i \frac{dS}{d\tau}, \quad \tau = \tau_{max}. \tag{I.4.4}$$

$\epsilon = \frac{\chi_s}{\chi_a + \chi_s}$, $d\tau = -(\chi_a + \chi_s)dz$, $S = \frac{j}{\chi_a}$ is the source function. I_{ei} is an external radiation, which is defined as:

$$I_{ei} = r_\mu^i I_{iso}, \tag{I.4.5}$$

where r_μ^i are weight coefficients, I_{iso} is an isotropic intensity . Thus, in case of an isotropic external radiation ($I(\mu) = I_{iso}$, at $\mu < 0$, otherwise $I(\mu) = 0$) $r_\mu^i = 1$ for any i. If an incident flux is considered as a global characteristic of the external radiation, then, in general case, r_μ^i are normalized in such a way that the flux is equals to the flux for isotropic distribution $I(\mu)$:

$$\sum r_\mu^i \mu_i w_i = 0.5 \tag{I.4.6}$$

The calculated values of V_i allow us to obtain two moments of the radiation field:

$$J = \sum_{i=1}^{3} V_i w_i \tag{I.4.7}$$

$$K = \sum_{i=1}^{3} V_i \mu_i^2 w_i, \tag{I.4.8}$$

To obtain the Eddington flux H, other combination should be considered:

$$U_i = \frac{I(\mu_i) - I(-\mu_i)}{2} \tag{I.4.9}$$

However, in practice, there is no need to solve again the differencial equation for U_i. Having J and K, the flux H can be calculated either by integration of the equation:

$$\frac{dH}{d\tau} = \chi_a (J - S), \tag{I.4.10}$$

with a boundary condition:

$$H_0 = \int (V_0 - I_e)\mu d\mu = \sum (V_{0i} - I_{ei})\, \mu_i w_i. \tag{I.4.11}$$

either by differentiation of the moment K :

$$H = \frac{dK}{d\tau}. \tag{I.4.12}$$

In case of an isotropic radiation field, the last expression reduces to the expression for the diffusion approximation $H = \frac{1}{3} dJ/d\tau$.

The comparison of both methods for a LTE-model of the star with $T_{eff} = 11000$ K, $\log g = 4.0$ has shown that the differential method leads to good enough results at every depth and frequency, while the integral method leads to absurd solutions at points with a very high opacity.

I.5. The temperature correction

The program uses four temperature corrections, three of them are summands of the Unsold-Lucy correction scheme, which has been modified by Dreizler (2003) to take into account departures from LTE. The first correction is designed for upper layers and can be applied for convective as well as non-convective models. The second and third corrections are the flux corrections and are designed only for non-convective models.

The fourth correction can be used in convective as well as non-convective models. It is Avrett-Krook temperature correction, which has been modified to include a convection. This part of the code was adopted from the ATLAS9 code (Kurucz, 1970; Castelli, Kurucz, 2004) with some changes due to differences in the method of a calculation of the convection. This correction are designed only for LTE case, but it is applied only for convective layers, where departures from LTE are negligible.

All the necessary integrals over the frequency are calculated at the last Λ-iteration (in a subroutine alinvel.f90). Referring for details to the cited works, we will only discuss here some questions that are still unclear.

I.5.1. The splitting of the source function into a thermal and non-thermal contribution

The temperature corection scheme in non-LTE case is based on the splitting of the source function into a thermal and non-thermal contribution, which is treated as a scattering:

$$\chi^a_\nu S_\nu = \kappa^B_\nu B_\nu + \gamma_\nu J_\nu. \tag{I.5.1}$$

If the relative difference between the source function of any non-LTE transition and the Planck function is less than δ_S, then the transition is classified as "thermal", else it is considered as "non-thermal". Test runs (see part III) have shown that the optimal value of $\delta_S = 10^{-2}$. The expression (I.5.1) implies that the "non-thermal" opacity sources are not dependent on temperature, therefore, the method will not work when the "non-thermal" opacity dominates. In such cases linearization methods should be applied.

I.5.2. The problem of slow convergence caused by the presence of spectral regions with a high opacity

The problem is as follows. The first temperature correction (Λ-correction), which operates in upper layers, can be written as follows:

$$\Delta T = \frac{\int \chi_\nu^a (J_\nu - S_\nu) d\nu}{\int \chi_\nu^a \frac{dS_\nu}{dT} d\nu}. \tag{I.5.2}$$

Let us decompose the integrals into the sum of integrals over spectral regions with high and low opacity:

$$\Delta T = \frac{\int\limits_{high\chi} \chi_\nu^a (J_\nu - S_\nu) d\nu + \int\limits_{low\chi} \chi_\nu^a (J_\nu - S_\nu) d\nu}{\int\limits_{high\chi} \chi_\nu^a \frac{dS_\nu}{dT} d\nu + \int\limits_{low\chi} \chi_\nu^a \frac{dS_\nu}{dT} d\nu}. \tag{I.5.3}$$

In the optically-thick frequency points $J_\nu - S_\nu = 0$, therefore, at $\chi_{high} \to \infty$

$$\Delta T = \frac{const + \int\limits_{low\chi} \chi_\nu^a (J_\nu - S_\nu) d\nu}{\infty + \int\limits_{low\chi} \chi_\nu^a \frac{dS_\nu}{dT} d\nu} \to 0. \tag{I.5.4}$$

The temperature correction goes to zero, while the heat balance is not reached:

$$\int\limits_{low\chi} \chi_\nu^a (J_\nu - S_\nu) d\nu \neq 0. \tag{I.5.5}$$

Hence we need to remove from the integrals the optically-thick frequencies, at which the balance is set automatically. Due to this reason at calculations of mean opacities κ_P and κ_J (see Dreizler's paper) we remove from integrals the frequencies, at which

$$\left| \frac{\chi_\nu^a J_\nu}{\eta} - 1 \right| < stemp. \tag{I.5.6}$$

Test runs shows that the optimal value of $stemp = 10^{-3}$.

The Λ-correction operates only in upper layers $\tau_{Ross} \lesssim 1$, in more deep layers the flux correction is applied.

II

Atomic data

This section describes the atomic data set for hydrogen and helium, which has been used in simulations of accretion spots on the surface of young stars.

II.1. Hydrogen

For test purposes, we will consider a few models of Hydrogen atom, which include all levels with the principal quantum number n up to N_{max}, where $N_{max} = 10, 15, 20, 25, 30$. The ionization enegry of each level is calculated using the Rydberg formula. At high temperatures, when $\chi^{t,i+1}/kT$ is not small, the omitted upper levels can make a significant contribution to the partition function in Saha equation and can lead to wrong results. In ATLAS9 this problem has been solved by inclusion all excited states up to the last level n, which is defined by comparison of the energy of electron in atom with the energy in the mean electric field in a plasma (Kurucz, 1970):

$$n \approx 80 \left(\frac{T_4}{N_{c14}} \right)^{1/4} Z_{eff}^{1/2},$$

where N_c is a number density of charged particles with effective charge Z_{eff}.

In the DETAIL code this levels can be taken into account by inclusion of so-called S-level. However, tests have shown that at the values of N_{max}, which are used here, changes in the partition function lead to a small changes in b-factors (see Fig. II.6).

Another problem associated with a finite number of levels in the atom is a big number of lines, which merge into continuum at the ionization threshold. Ignoring these lines leads to decrease the opacity, that can be compensated by lowering the ionization threshold (see Fig. II.8). Thus, the missed opacity in lines is compensated by the continuous opacity. The same procedure allows us to account roughly the Stark wings of the photoionization cross-section (see Lin, Ho, 2011). Tests shows that lowering the ionization threshold allows to obtain results for a small N_{max}, which are close to the results for models with a big N_{max}.

Therefore, by default, ionization energies of the levels are calculated as follows:

$$E_{H\,I} = R_H \left(\frac{1}{n^2} - \frac{1}{(N_{max}+1)^2} \right), \tag{II.1.1}$$

The oscillator strengths are calculated by using the formulae from Berestetskij et al. (1989) and are well agree with data from NIST. Stark broadening was calculated for line profiles corresponding to the transitions from $n = 1 - 4$ to overlying levels: the tables of Stehle&Hutcheon (1999) were used for the transitions from $n = 1 - 3$ to $n \leq 7$, the theory

of Griem (1960) as implemented by Auer&Mihalas (1972) was applied for the rest lines with a lower level $n = 1 - 4$. Taking into account a big number of lines in the atomic model and Shark broadening for lines near series limits are necessary to reproduce real shapes of stellar spectra near the ionization threshold. Otherwise, the integral flux can be erroneous that leads to errors in the model of the atmosphere.

The rest lines are included, assuming Doppler profiles. For all lines the approximation of the complete frequency redistribution was assumed.

Electron-impact excitation rates are calculated as in PB04 (Przybilla&Butler, 2004) and correspond to model E from this paper. Model F will be used here only for comparison purposes.

Electron-impact ionization rates are evaluated according to Johnson (1972).

Photoionization cross sections and the f-f opacity are calculated applying hydrogenic expressions (Mihalas, 1978) with Gaunt factor g_{II} as in PB04.

In this part we will mark the atomic data set as follows: XN_{max}ShY, where X assumes values E or F for electron-impact excitation rates. N_{max} is the number of levels in the atomic model. The models with a shift of ionization thresholds are labeled by Sh, Y assumes values E, if the energies of levels are shifted, and P, if the thresholds of Photoionization are shifted, but the energy of levels for other processes are unchanged.

II.1.1. Tests

The original DETAIL code was used for the testing of the atomic models. The code allows to calculate departures from LTE for a few user-defined elements at a fixed atmospheric structure. The program provides a variety of methods to include the line-blanketing effect. The main method in our calculations is the Opacity Sampling (OS). However, in order to compare with results of old papers, we will use ODF method, which has a various implementations in the code: ODF BIG or ODF LIT Kurucz ODFs with large (BIG) or small (LIT) frequency steps; the original Kurucz treatment (KUR) or a less accurate, faster mean opacity version (AVE). ODF can be applied for non-LTE calculations only for hydrogen and helium, because all other elements are included in ODF in LTE approximation.

In order to test atomic data set for hydrogen, the calculations for the star β Ori, which is considered in detail by PB04, are reproduced. The atmospheric parameters of the star: $T_{eff} = 12000$ K, $\lg g = 1.75$, helium abundance $Y = 0.13$. Stark broadening of all lines with lower level $n \leq 4$ is calculated by applying the theory of Griem (1960). The velocity of microturbulence used in PB04 $V_{mic} = 7$ km s^{-1}. I have not the ODF file for this microturbulence, moreover Przybilla and Butler have used the old ODF files, which are no longer available. However, we can easily evaluate the effect of turbulence on b-factors by using the opacity sampling technique. The departure coefficients as a function of Rosseland optical depth τ_{Ross} are shown on Fig. II.1 for the model E30ShE and two values of the microturbulence $V_{mic} = 1$ and 7 km s^{-1} .

A comparison of OS and ODF methods for the same model with $V_{mic} = 1$ km s^{-1} is shown on Fig. II.2. It can be seen that only the first and second levels are strongly dependent on the method, which was used.

It has been found in PB04 that the result depends on the number of levels in the atomic model. Our results for the atomic models E(10,20,30)ShE have not shown similar dependence (see. Fig. II.3) A 20-level model leads to the same results as a 30-level model. A 10-level model shows a little differences.

In the models E(10,20,30) without the lowering of ionization energy the dependence on

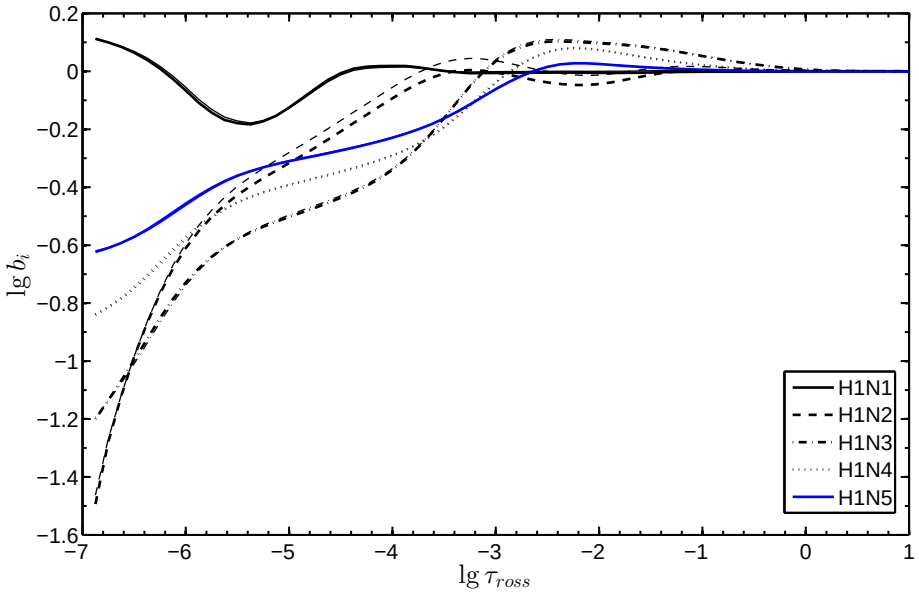

Figure II.1: b-factors of hydrogen levels. OS with $V_{mic} = 7$ km s^{-1} (the thick curves) and $V_{mic} = 1$ km s^{-1} (the thin curves). A notable difference can only be seen for $n = 2$. Atomic model: E30ShE

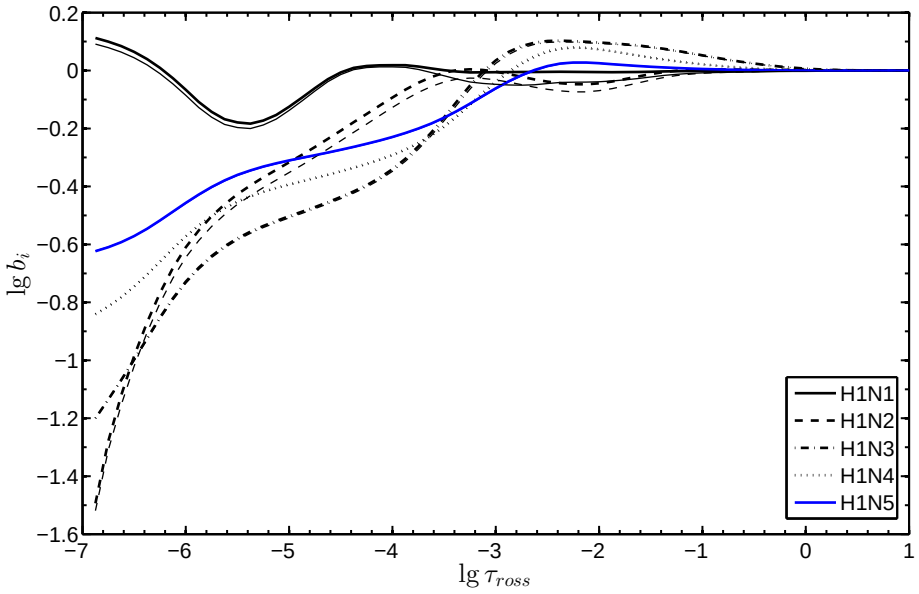

Figure II.2: The departure coefficients for hydrogen levels calculated with OS (the thick curves) and ODF AVE BIG (the thin curves). $V_{mic} = 1$ km s^{-1}. E30ShE

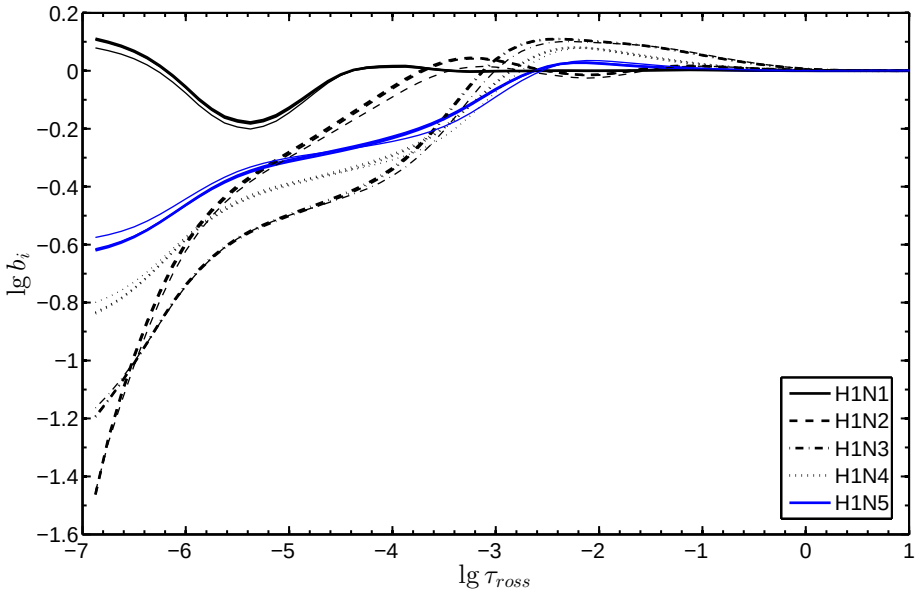

Figure II.3: b-factors of hydrogen levels for the atomic data sets E(10,20,30)ShE. Thicker lines correspond to a bigger atom. The lines for 20-level and 30-level models are practically coincide. OS. $V_{mic} = 7$ km s^{-1}.

the number of levels is considerably increased (Fig. II.4). This effect is primarily associated with the location of the photoionization threshold, thus, if we reduce only the frequency of the photoionization threshold, then the dependence is absent again (Fig. II.5).

The inclusion of additional levels in the form of S-level does not impact on the results, any changes in the departure coefficients are less than 1% (see Fig. II.6).

The differences in the level populations in the E and F models are shown on Fig. II.7.

In general, the behaviours of the departures from LTE in our tests and in PB04 are similar, but the scale of the departures in our tests turns smaller than in PB04. It probably caused by differences in ODF files (old and new ODF) as well as in the model of the atmosphere.

The differences of radiation fields obtained in the atomic models with and without the lowering of the photoionization threshold are shown on Fig. II.8. The area bounded by the red and black curve is the radiation, which is missed in the photoionization process in the models without the lowering. However, the lowering is first and a very rough approximation for a simulation of the Stark wings of the photoionization cross-section. The jump at the series limit is artificial and caused by the sharp edge of the photoionization cross-section. The shift of the threshold allows us to take into account the main effect.

To construct an accurate model of the stellar atmosphere, the total flux should be calculated accurately, therefore the Stark wings of all distinguishable hydrogen lines as well as the Stark wings of the photoionization cross-section should be taken into account.

There are an alternative method for a calculation of the spectrum near series limits. To make a smooth transition from the lines to the continuum, a dummy line, labeled in the line list as CONTINUUM, is put at the frequency of the ionization threshold in the SYNTHE code. In a similar way the problem is solved in the TLUSTY code, where the atomic model contains 8 levels + "merged"-level. Thus, the last Balmer line, which is explicitly calculated in the TLUSTY code, is 3890Å(vac), and all higher members are treated as a pseudo-

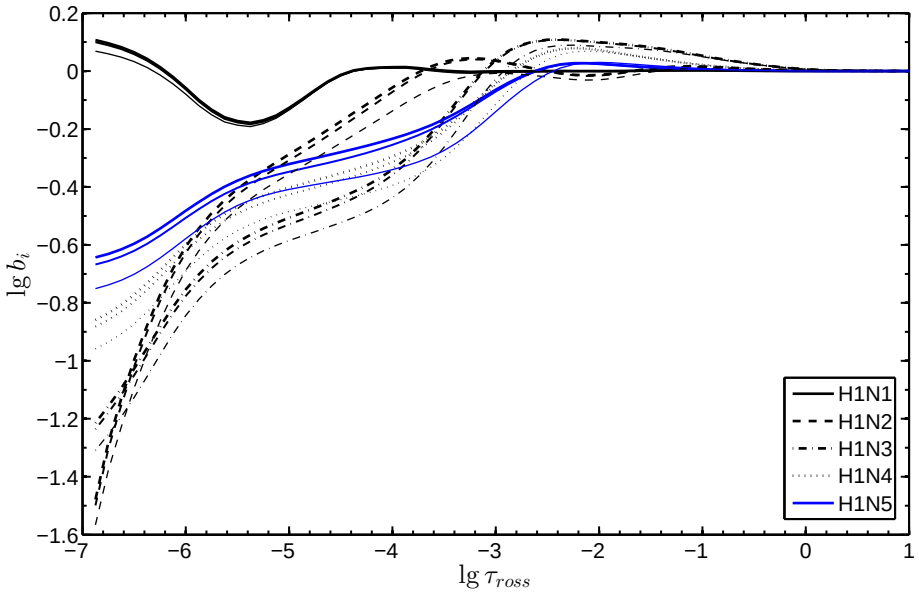

Figure II.4: b-factors of hydrogen levels. Atomic model is E(10,20,30), i.e. without the lowering of ionization energy. OS. $V_{mic} = 7$ km s^{-1}.

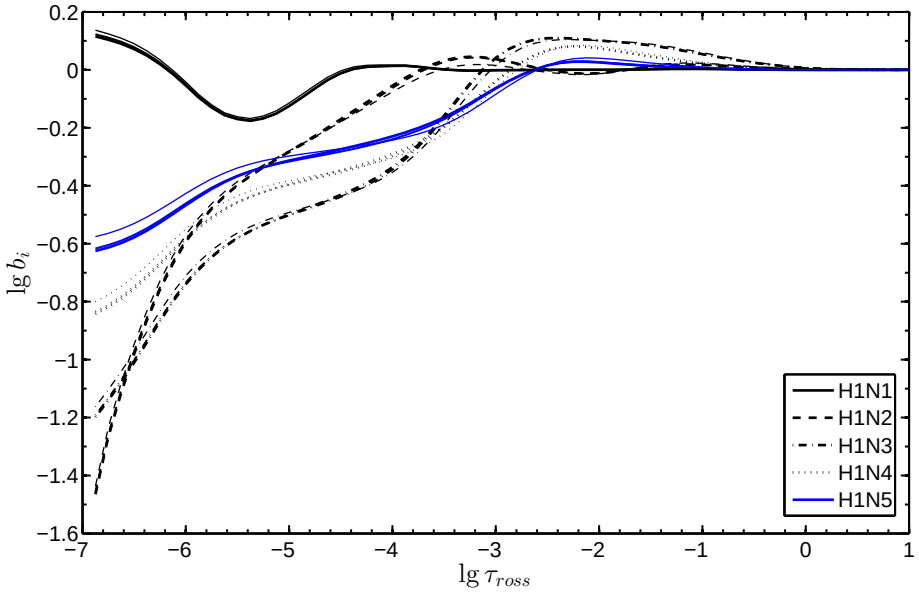

Figure II.5: b-factors of hydrogen levels. Atomic model is E(10,20,30)ShP, i.e. the frequency of the photoionization threshold is reduced, but the ionization energies (for example, in case of a collisional ionisation) correspond to the Rydberg formula without any changes. OS. $V_{mic} = 7$ km s^{-1}.

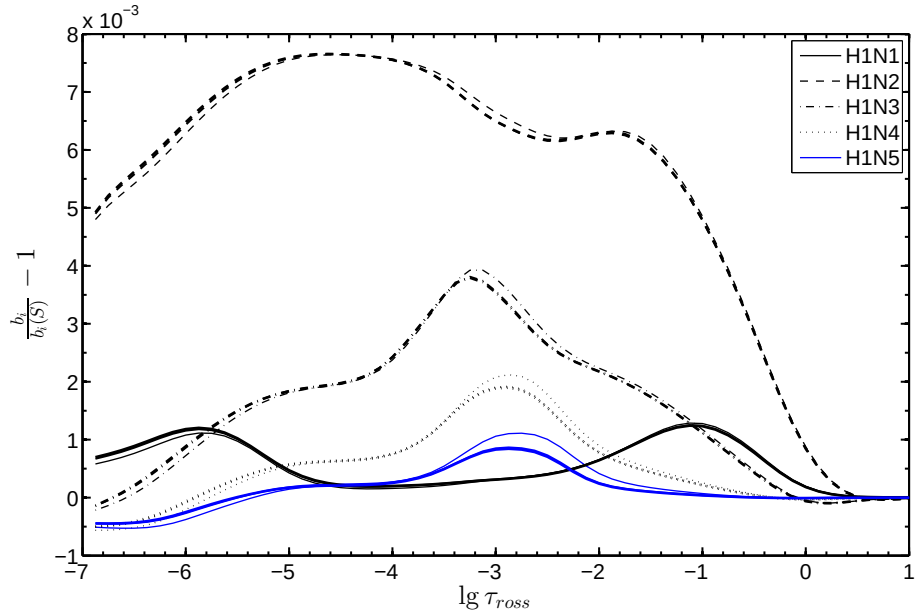

Figure II.6: The relative difference of b-factors for hydrogen levels in the models with various number of levels E(10,20,30) with and without the S-level. The thin line corresponds to $N_{max} = 10$. OS. $V_{mic} = 7$ km s^{-1}.

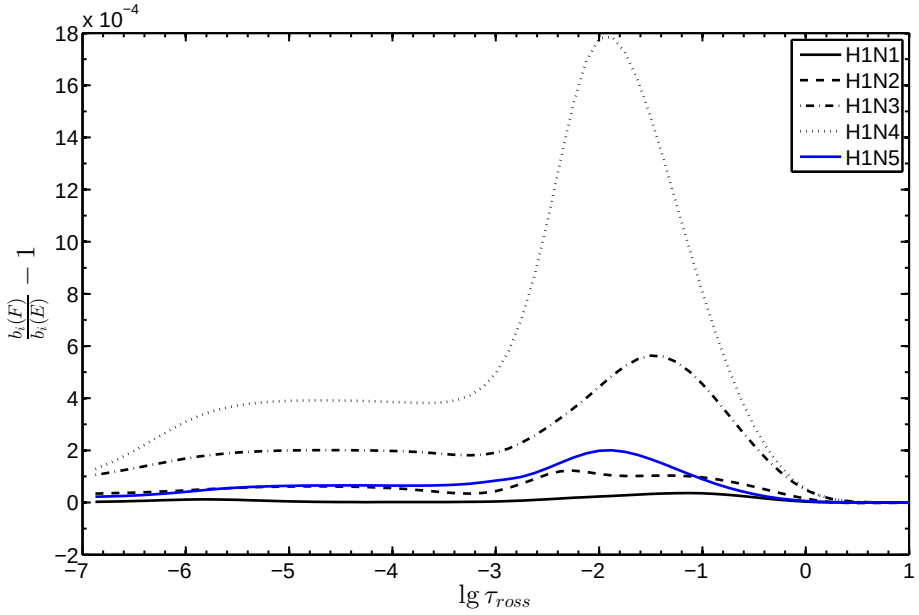

Figure II.7: The relative difference of b-factors for hydrogen levels in the E and F models from PB04. Atomic models: E30ShE and F30ShE. OS. $V_{mic} = 7$ km s^{-1}.

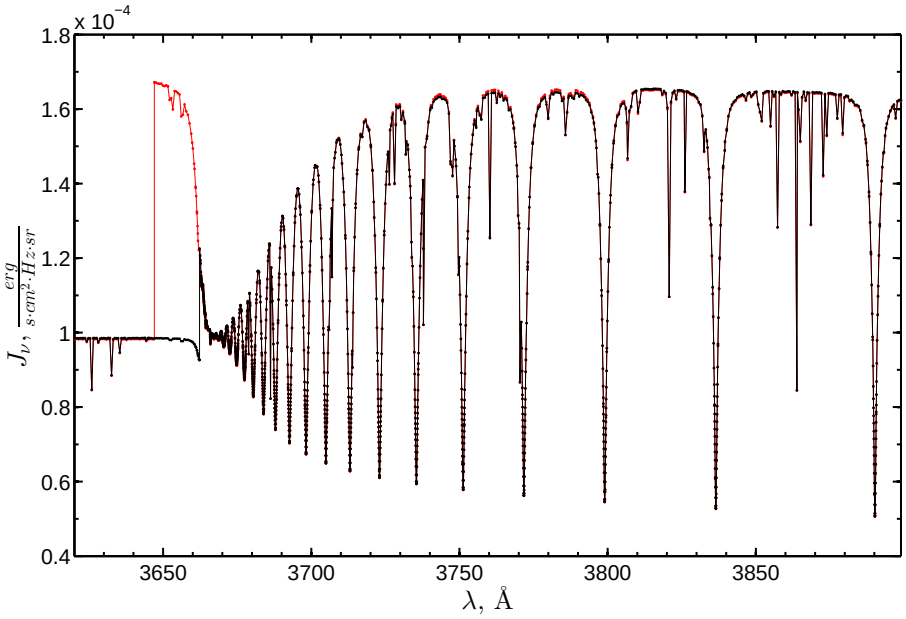

Figure II.8: The radiation field J_ν near the Balmer jump. $N_{max} = 30$. The black curve corresponds to the model with the lowering of the ionisation energies (E30ShE). The red curve – without the lowering (E30). $V_{mic} = 7$ km s^{-1}.

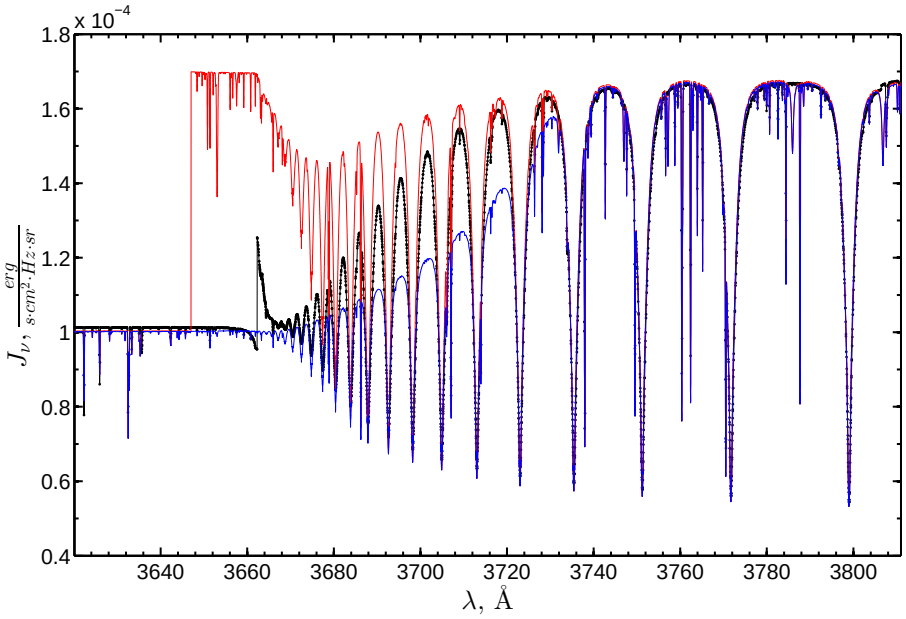

Figure II.9: The radiation field J_ν near the Balmer jump. $N_{max} = 30$. The black curve corresponds to our calculations: OS, 30 000 frequency points between 100-10000Å. The red curve is calculated in SYNTHE without the line labeled as CONTINUUM, the blue curve – with this line. The spectral resolution is 600 000. $V_{mic} = 7$ km s^{-1}.

continuum (Hubeny et al., 1994). In future, the line like CONTINUUM can be introduced in the code as a part of the photoionization cross-section.

II.2. Helium

II.2.1. He I

Two models of the helium atom are considered. Both models include all states up to principal quantum number $N_{max} = 10$. Energies of levels are adopted from the NIST database, and reduced on an energy of the levels with $n = 11$ as it was done before, in the case of hydrogen atom. In one model all states up to $n = 5$ are treated individually, as it was done in P05 (Przybilla, 2005), while in other model all states up to $n = 7$ are treated individually (see Fig. II.10 II.11). The remainder states are grouped into combined levels for each n in the singlet and triplet spin systems.

Wavelengths and oscillator strengths of spectral lines are adopted from the NIST database and supplemented by data from the NORAD database (Nahar, 2010). Stark broadening is accounted for using the tables of Dimitrijevic, Sahal-Brechot (1984). Lines, which have not been included in the tables, are calculated, assuming Doppler profiles. Many helium lines have a multicomponent structure, which leads to a significant broadening and distortion of the profiles. Hence the profile is calculated as a weighted mean over all components of the thin structure:

$$\varphi(\lambda) = \frac{\sum g_i f_i \phi(\lambda - \lambda_i)}{\sum g_i f_i},$$

where ϕ is the profile of i-th component with a wavelength λ_i and gf-value $g_i f_i$.

Electron-impact excitation rates for all transitions from $n = 1, 2$ (except $2p\,^1P$) to $n = 2 - 5$ are adopted from Bray et al. (2000). Additional transitions are treated according to Mihalas & Stone (1968) and for the remainder of the optically forbidden transitions, the semiempirical Allen formula (Allen, 1973) is applied.

Collisioanl ionization is accounted for according to Mihalas, Stone (1968).

Photoionization cross-sections for all levels with $n \leq 7$ are adopted from the NORAD database (Nahar, 2010). These cross-sections for the levels $1s^2\,^1S$ and $2s\,^3S$ well agree with the cross-sections from Fernley et al. (1987), which were used in P05 (see Fig. II.12-II.14). The cross-sections for the levels with $n = 6 - 7$ in the atomic data set N10l5 are averaged with a statistical weight g over the combined sublevels

Photoionization cross sections for the levels with $n = 8 - 10$ are evaluated applying hydrogenic expressions. The averaged cross-sections from the NORAD database agree with the hydrogenic cross-sections better than 25% for $n = 6$ and better than 20% for $n = 7$. Thus, it can be expected that for $n > 7$ the agreement will be better than 20% at the threshold.

II.2.2. He II

The model of He II atom includes all states up to principal quantum number $N_{max} = 20, 40$. The energy for each state is defined in a similar way as for hydrogen (see Eq. II.1.1):

$$E_{He\,II} = 4R_{He}\left(\frac{1}{n^2} - \frac{1}{(N_{max}+1)^2}\right). \qquad \text{(II.2.1)}$$

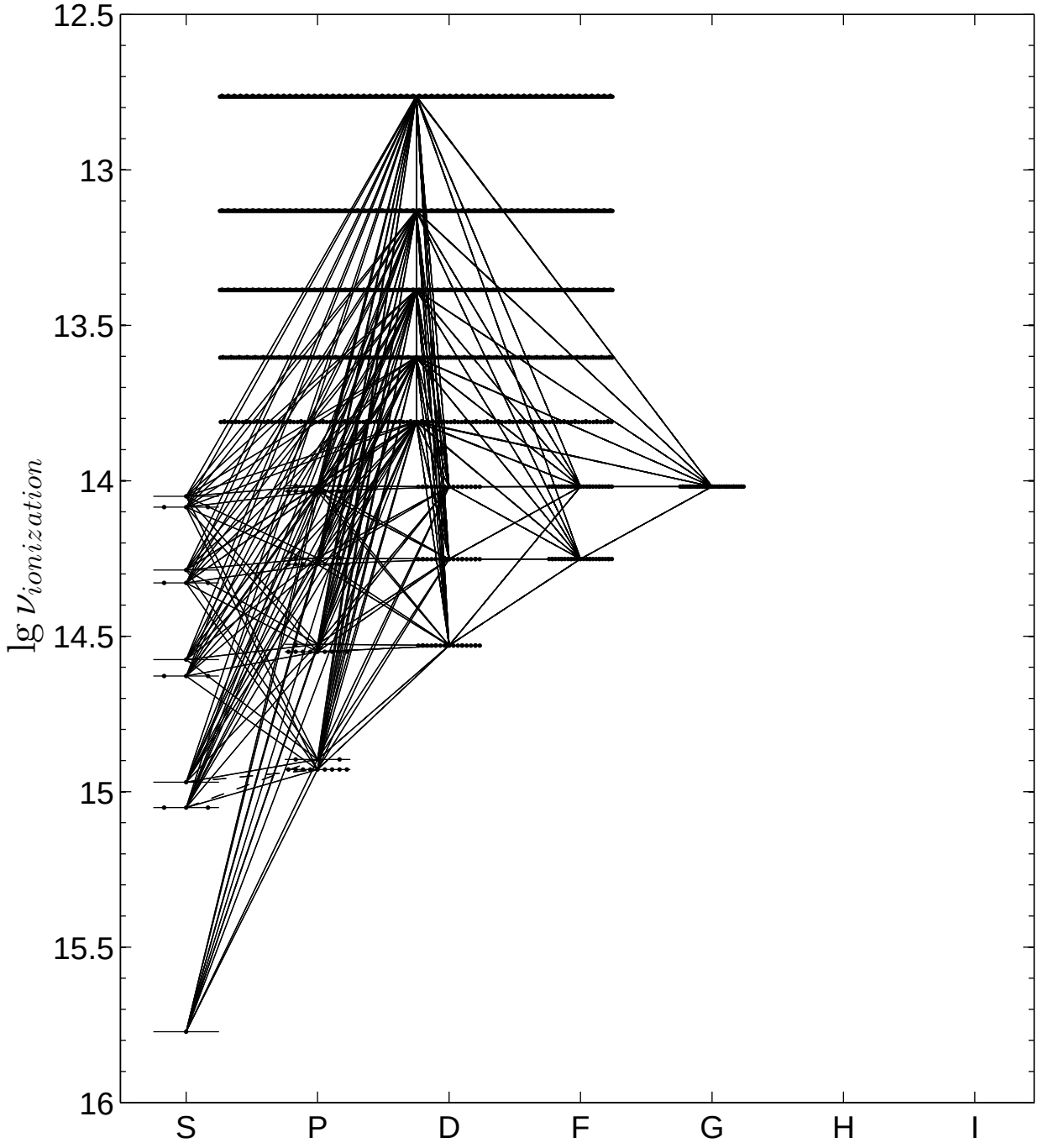

Figure II.10: The model of helium atom N10l5. Atomic levels and radiative transitions considered in the model are shown.

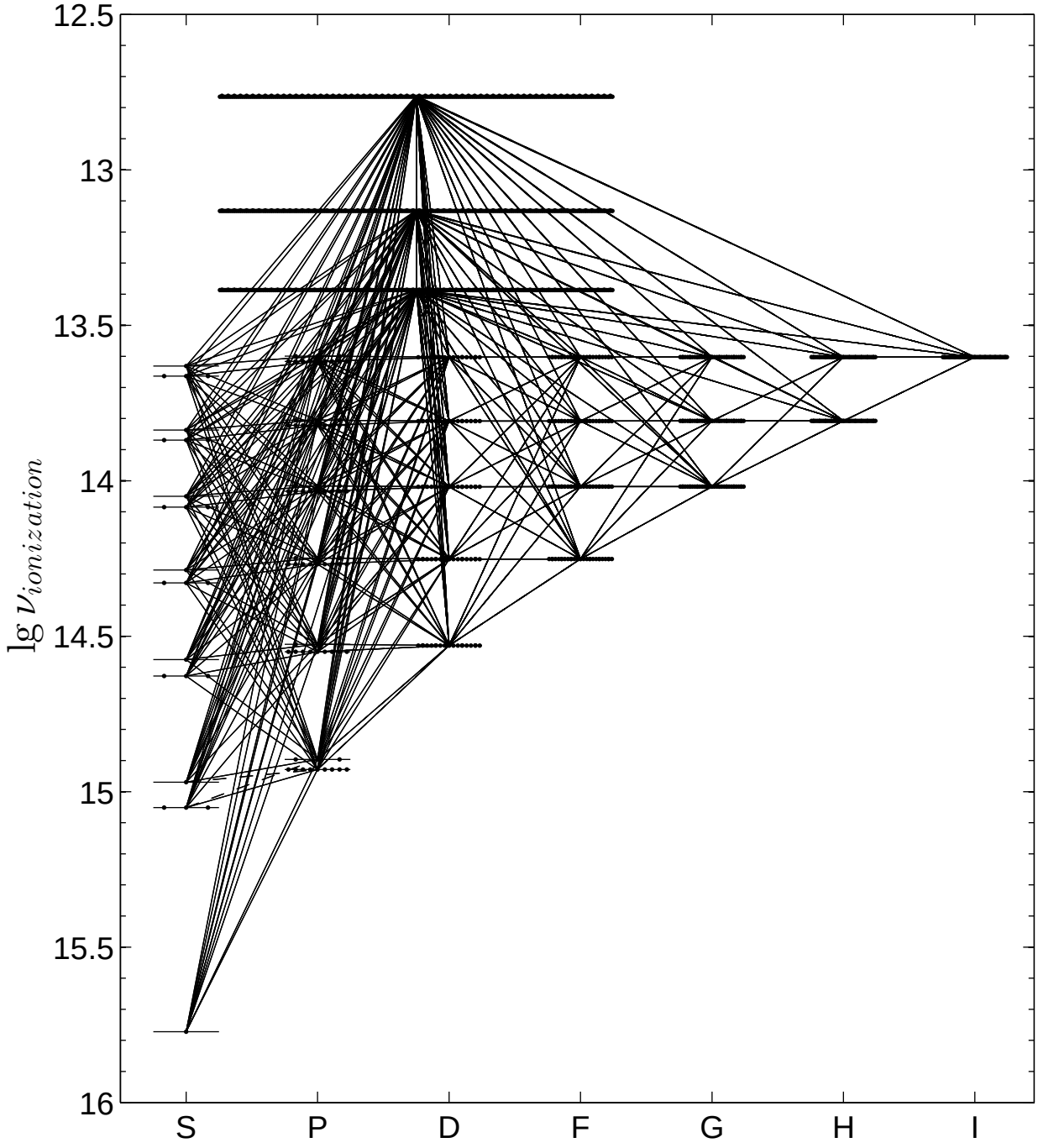

Figure II.11: The model of helium atom N10l7. Atomic levels and radiative transitions considered in the model are shown.

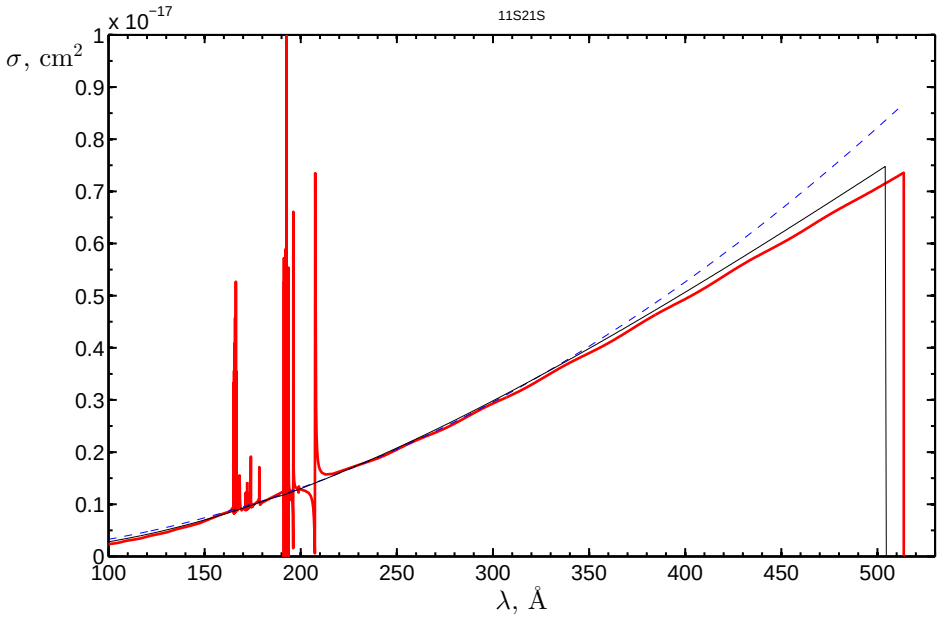

Figure II.12: Photoionization cross-section of He I $1s^2\,{}^1S$. The black curve corresponds to the cross-section, which was used in P05 (Fernley et al. 1987, without autoionization resonances). The red line corresponds to the cross-section from NORAD. In the NORAD data the ground state has smaller ionization energy by 1.8%. A difference at the threshold $\sim 4\%$. The blue dashed line corresponds to the cross-section taken from the ATLAS9 code.

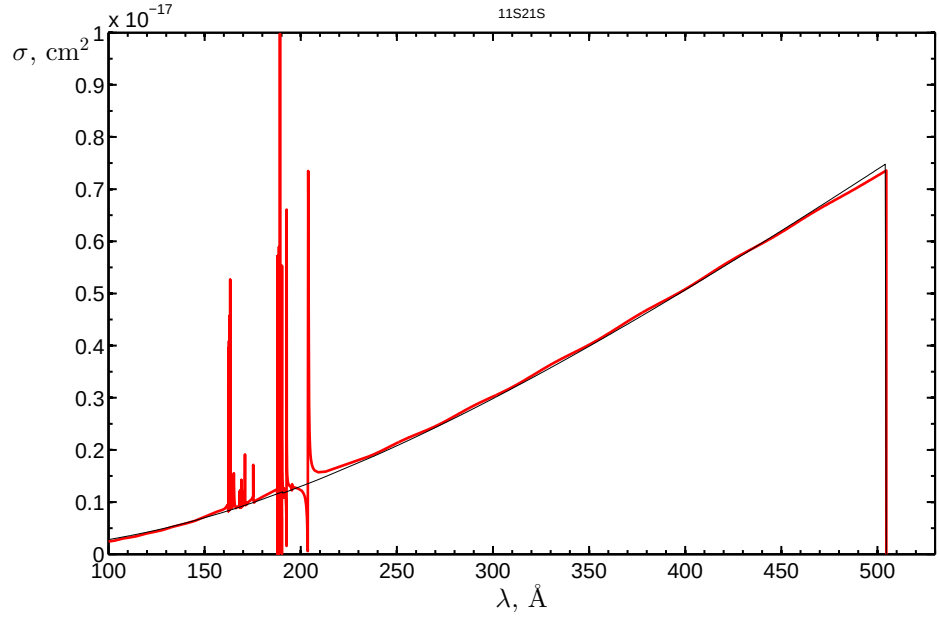

Figure II.13: The same as in Fig. II.12, but for the cross-section from NORAD with corrected frequencies by 1.8%.

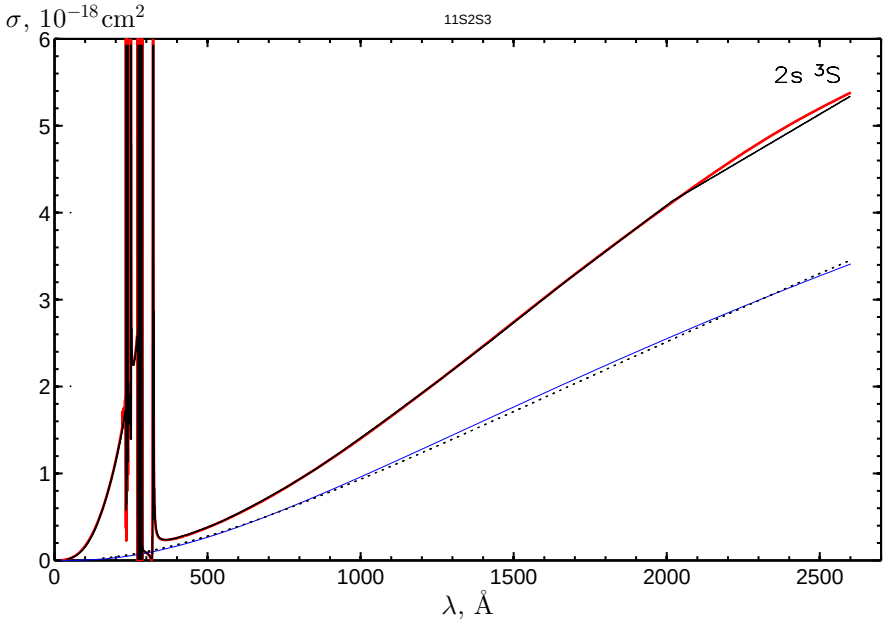

Figure II.14: The black curve corresponds to the photoionization cross-section, which was used in P05 for the $2s^3S$ state. The black dashed curve corresponds to the "old" cross-section. The red curve is for the NORAD cross-section. A difference at the threshold $\sim 0.75\%$. The blue line is for the cross-section taken from the ATLAS9 code but **multiplied by a factor of 16!**

Oscillator strengths are hydrogenic. Stark broadening was calculated for line profiles corresponding to the transitions from $n = 1 - 4$ to overlying levels using the theory of Griem (1960) as implemented by Auer and Mihalas (1972). The rest lines are included, assuming Doppler profiles. For all lines the approximation of the complete frequency redistribution was assumed.

Electron-impact excitation rates for all transitions from $n = 1, 2$ to $n = 2-5$ are adopted from the CHIANTI database (Dere et al., 1997, Landi et al., 2006). The theory of Percival and Richards (1978) is applied for the transitions between levels with $n \geq 5$. A scaled fit to Sampson & Golden (NCAR-76, Mihalas 1972) is used for the rest transitions.

Electron-impact ionization of the levels with $n \leq 7$ is accounted for according to Clark et al. (1991) and for the remainder levels, the Seaton (1962) approximation is applied.

Photoionization cross-sections for He II are calculated applying hydrogenic expressions (Mihalas, 1978) with Gaunt factor g_{II} as in PB04.

II.2.3. Tests

To test the data sets for helium, the results of P05 were reproduced. The stellar parameters are $T_{eff} = 30000$ K, $\lg g = 4.0$, solar elemental abundances. The microturbulence velocity is $V_{mic} = 1$ km s^{-1}, however the presented results are not changed, if $V_{mic} = 0$ km s^{-1} are used.

Hydrogen are calculated in the test in LTE approximation with the atomic data set labeled as E20ShE.

The behaviours of the departures from LTE in our model and in P05 are similar, however there are some differences, especially in the population of the ground state. We managed to roughly halve the magnitude of these differences (see Fig. II.15), replacing the OS method

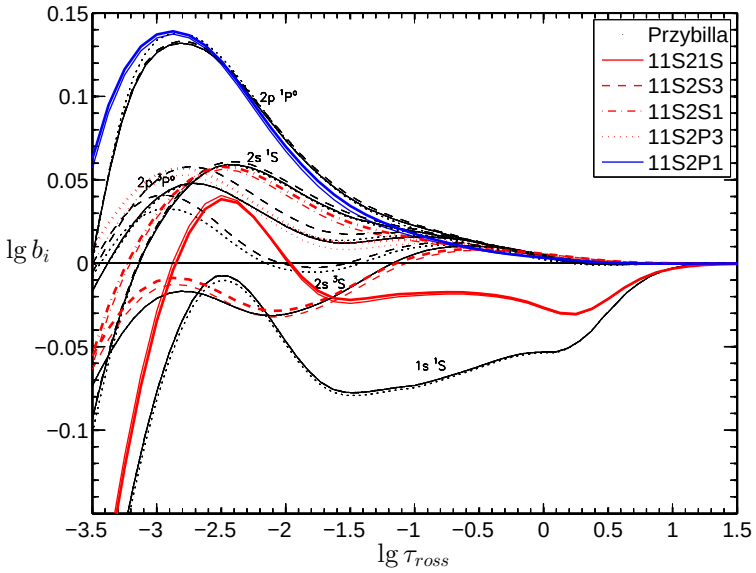

Figure II.15: Comparison of departure coefficients as a function of Rosseland optical depth τ_{Ross} for $n = 1, 2$ levels of He I from our computations (color lines) and from P05 (black lines and dots). Atomic model is N10l5. Line-blanketing is accounted for using ODF AVE BIG. The thick and thin lines correspond to the models with and without the lowering of ionization enirgies. $V_{mic} = 0$ km s^{-1}.

by the ODF method, which has been used in P05. Final residuals in the b-factors of the ground state are less than 10%. Perhaps the differences can be explained by different versions of the DETAIL code and by different versions of ODF files, because Przybilla (private communications) has used old ODF (Kurucz, 1990), which are unavailable now, and we were forced to use the new ODF (Castelli&Kurucz, 2004).

In addition to the differences in the methods, accounting for the line-blanketing effect (to compare results obtained with OS and ODF, see Fig. II.16), a treatment of photoionization opacities of LTE-elements is not described in P05. However, there are a number of photoionization thresholds of the various elements, which alter the spectrum significantly in the region 200-400Å(see Fig. II.17 and II.18).

For test purposes we use the photoionization cross-sections, that are similar to the cross-sections used in the ATLAS9 code, however the recent data leads to very similar spectrum (see Fig. II.18). The omission of this opacity results in slight enhancement of the departures from LTE for the ground state (see Fig. II.19).

The figures II.20 – II.22 provide some additional tests (different atomic models, an impact of the microturbulence).

II.3. LTE-elements

To calculate the line-opacities by the opacity sampling technique, the models of atoms and ions were defined for the following elements: C I-V, N I-VI, O I-VII, F I-VIII, Ne I-IX, Na I-X, Mg I-IX, Al I-VIII, Si I-IX, P I-VII, S I-VIII, Cl I-VIII, Ar I-IX, K I-X, Ca I-XI, Sc I-XII, Ti I-XIII, V I-XI, Cr I-XI, Mn I-XI, Fe I-X, Co I-X, Ni I-XI, Cu I-XII, Zn I-XI. It turns out that this is enough for modeling stars with temperatures T_{eff} up to $\sim 30\,000$ K

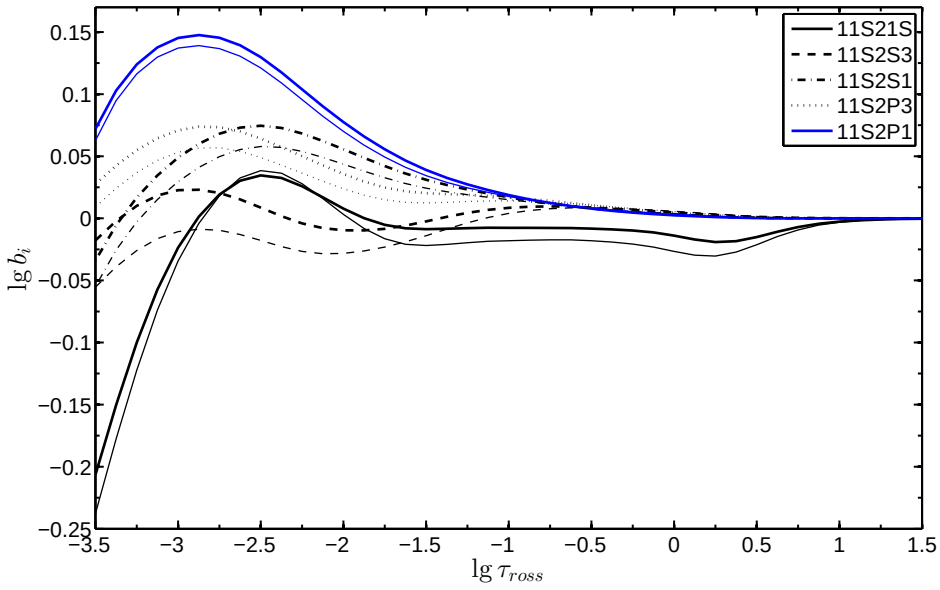

Figure II.16: Departure coefficients as a function of Rosseland optical depth τ_{Ross} for $n = 1, 2$ levels of He I. The line-blanketing effect is accounted for using the OS technique (the thick curves) and ODF AVE BIG (the thin curves). Atomic model is N10l5. $V_{mic} = 0$ km s^{-1}.

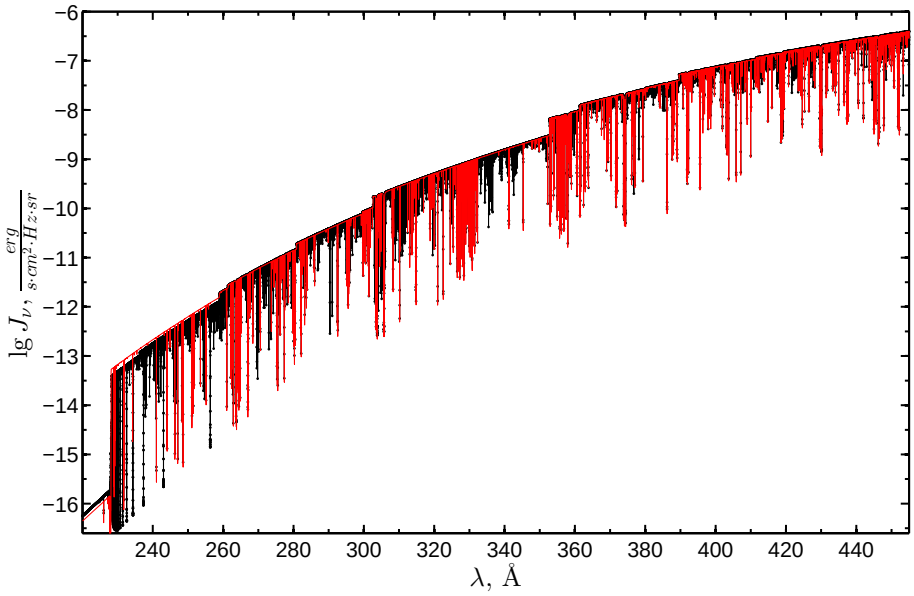

Figure II.17: Comparison of radiation fields calculated with DETAIL (the black curve) and SYNTHE (the red curve) at 200-400Å, where a number of photoionization thresholds are placed. The photoionization cross-sections used in the DETAIL run are adopted from the compilation by Golovatyj et al. (1997). $V_{mic} = 0$ km s^{-1}.

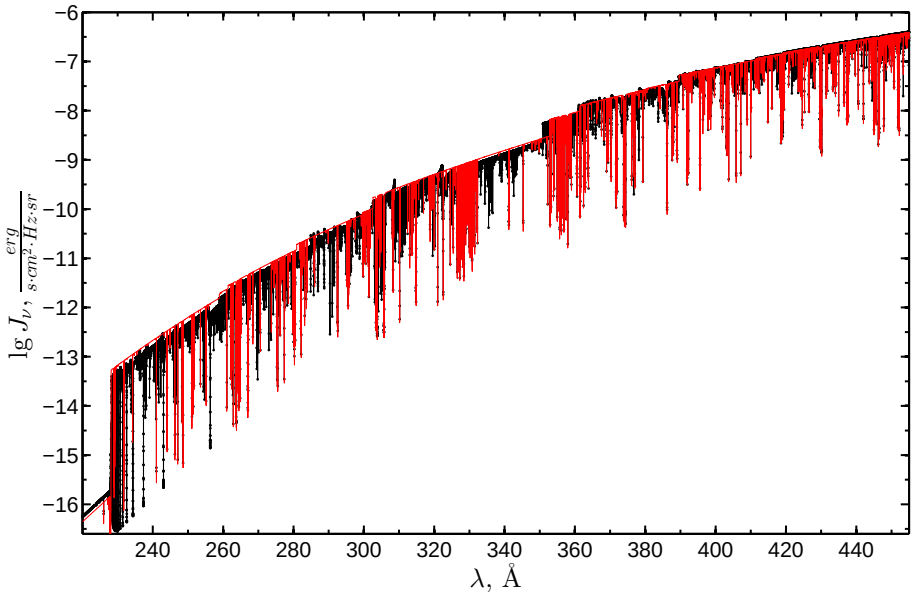

Figure II.18: Comparison of radiation fields calculated with DETAIL (the black curve) and SYNTHE (the red curve) at 200-400Å, where a number of photoionization thresholds are placed. Here we have used the recent photoionization cross-sections from the Opacity Project (TOPBase). $V_{mic} = 0$ km s^{-1}.

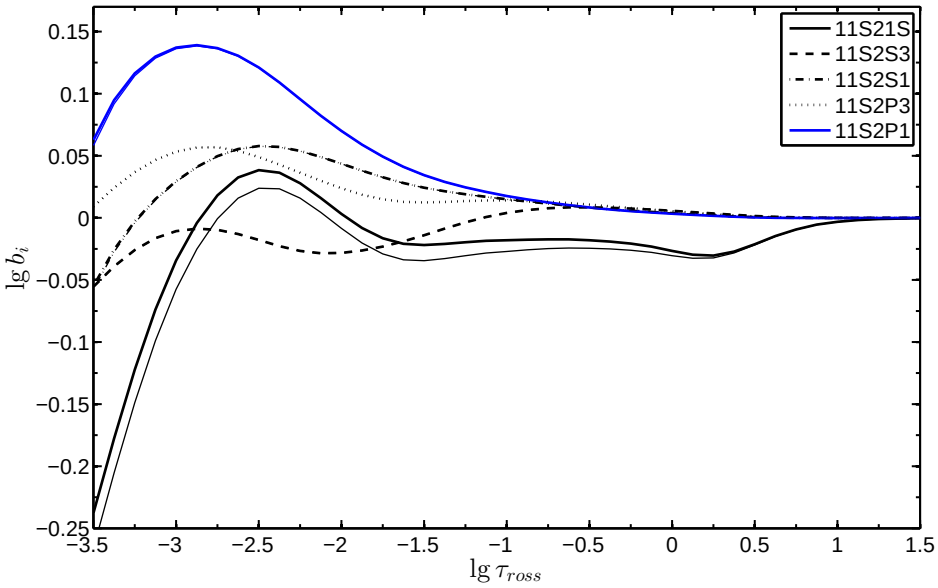

Figure II.19: Departure coefficients as a function of Rosseland optical depth τ_{Ross} for $n = 1, 2$ levels of He I in the model of N10l5. ODF AVE BIG. The thick and thin curves correspond to the calculations with and without the inclusion of additional opacity sources between 200-400Å. $V_{mic} = 0$ km s^{-1}.

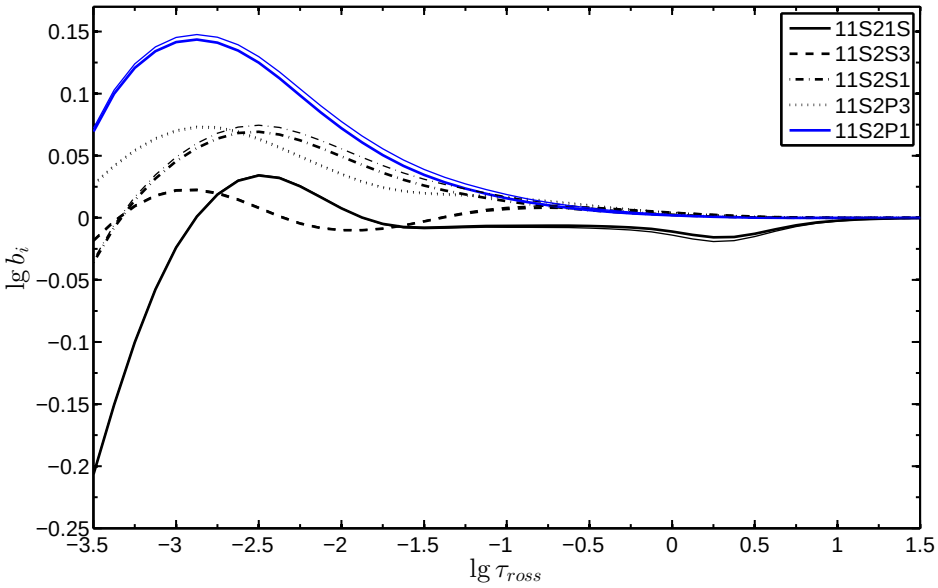

Figure II.20: Departure coefficients as a function of Rosseland optical depth τ_{Ross} for $n = 1, 2$ levels of He I in the model of N10l7 (the thick curves) and N10l5 (the thin curves). OS. $V_{mic} = 0$ km s^{-1}.

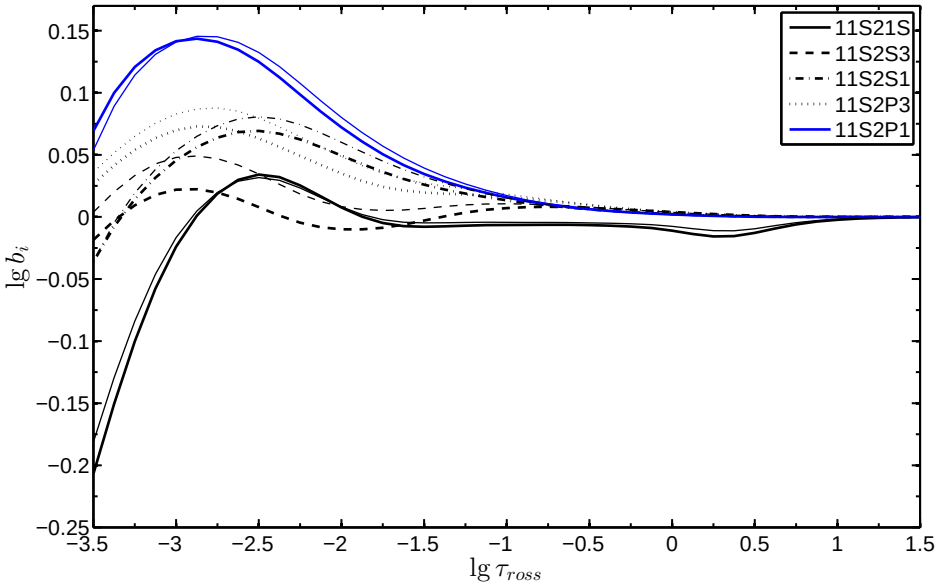

Figure II.21: Comparison of departure coefficients calculated for two values of the microturbulence velocity: $V_{mic} = 0$ km s^{-1}. (the thick curves) and $V_{mic} = 8$ km s^{-1}. (the thin curves). N10l7. OS.

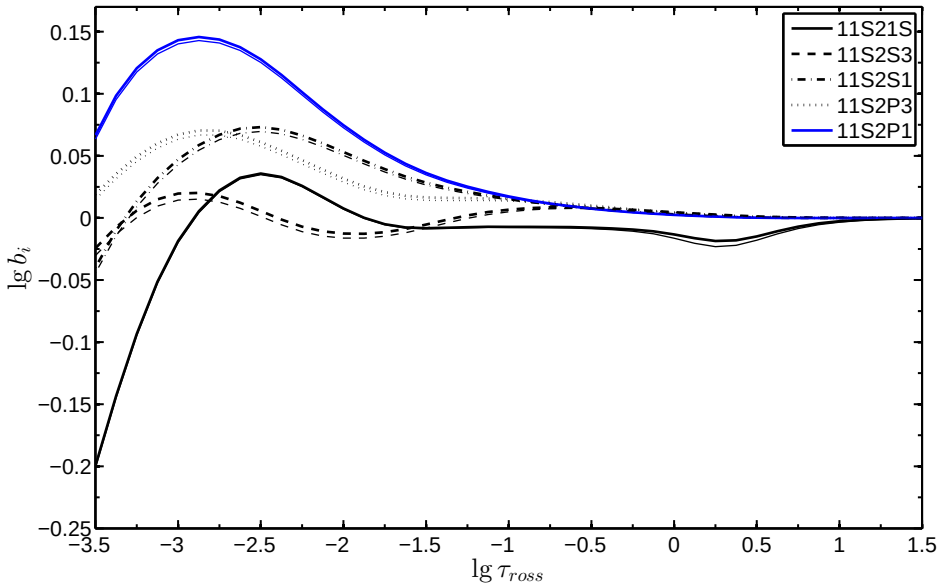

Figure II.22: Comparison of departure coefficients calculated for the model without the lowering of ionization energies (the thick curves) and for the model with S-levels, which combine the levels with n =11-180 for He I, with n =41-260 for He II and with n =21-180 in case of H I. OS, N10l5.

To reduce the CPU time, the ions with relative concentration[1] less than 10^{-10} are ignored.

The atomic models should include a sufficient number of states, to calculate the partition function in Saha equations with desired accuracy. Energies and statistical weights of the states are adopted from the NIST database. States with close energies are grouped in one level.

Since we certainly cannot include all possible levels, the partition function is calculated correctly only if $E_{ion} \gg kT$. If this condition is not satisfied, the considered ion must be highly ionized, and therefore it cannot give a large contribution to the total opacity.

Photoionization cross-sections from ground and excited states are adopted from the Opacity Project (TOPBase) for the following elements and ions: C I-IV, N I-V, O I-VI, Ne I-VI, Mg I-VI, Al I-VII, Si I-VI, S I-VII, Ar I-VIII.

[1] The ratio of the concentration of the ion to the concentration of atomic nuclei in all atoms and ions.

III

Tests

III.1. Stellar atmospheres without an external irradiation

To test our code for modelling of stellar atmosphere, we consider a stellar model with parameters $T_{eff} = 11\,000$ K, $\lg g = 4.0$.

The models are calculated for zero-metallicity in LTE and non-LTE in our program and in the TLUSTY program. It allows to find out how the different approaches, atomic models and atomic data for hydrogen and helium impact on the structure of the stellar atmosphere. It turned out that the LTE models are well agree, but non-LTE models shows a difference at the uppermost layers $\log \tau_{Ross} < -5.5$ (see Fig. III.1). It turned out that in these layers the temperature correction scheme does not work properly (see corresponding section) and the balance between heating and cooling cannot be reached. This is the only case when some linearization methods should be applied, because the heat balance of uppermost layers of hydrogen-helium star is defined by non-LTE-elements. Such extreme cases can be easily discarded by checking the heat balance. The non-LTE models calculated with TLUSTY and our code are well agree at the depths, where the iteration process of the temperature corrections converges well.

The stellar atmosphere with the same parameters is calculated for solar elemental abundances in ATLAS9 and in our program (see Fig. III.1). This test allows to check the correctness of our treatment of LTE-elements. It can be seen from the figure that the results obtained in both programs are well agree. Departures from LTE for hydrogen and helium do not result in strong changes in the atmospheric structure that is typical for stars of this kind (Hauschildt et al., 1999).

Comparison of the model calculated with ATLAS9 with our model, calculated with 30 000 frequency points in OS, shows that our model are cooler by 100-250 K at $\tau_{Ross} < 10^{-6}$ than the ATLAS9 model, which was calculated with ODF. The discrepancy disappears by increasing the number of points to 60 000.

The test shows that the models do not depend on the parameter *stemp* in the range from 10^{-2} to 10^{-8}. According to our definition of *stemp*, frequencies, at which the heat balance is satisfied with an accuracy $<$ *stemp*, are removed, therefore, a high value of *stemp* results to violate the heat balance. Thus, high values of *stemp* are inappropriate, while too small values of *stemp* result to a slow convergence. Tests shows an agreement better than 50 K with other programs in case of LTE models (LTE and non-LTE approaches are equivalent to test the parameter *stemp*).

To estimate the optimal value of the parameter δ_S, which is used only in non-LTE-

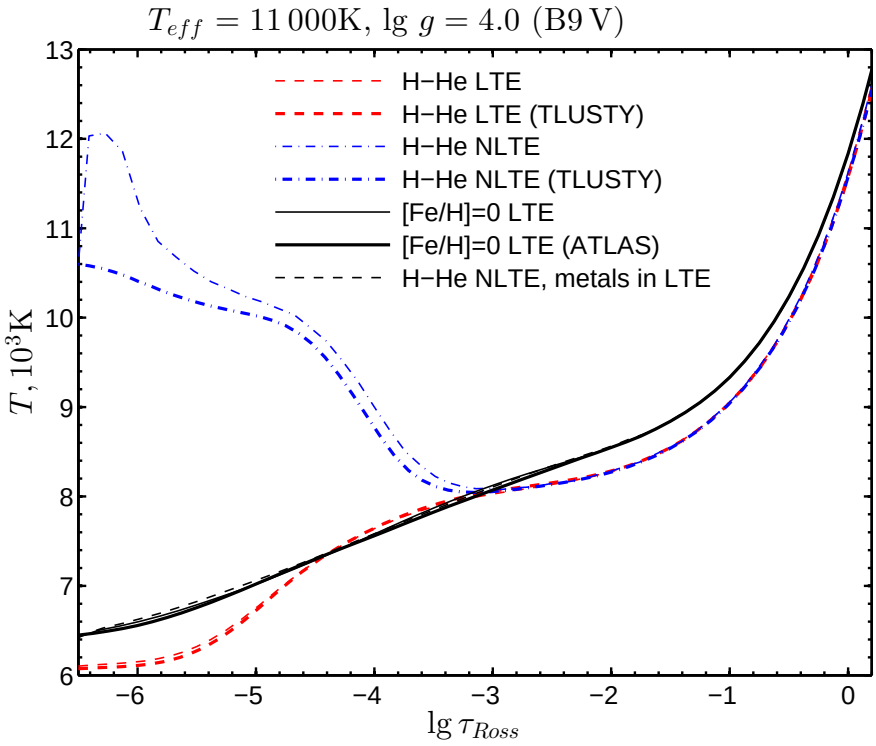

Figure III.1: Temperature as a function of Rosseland optical depth τ_{Ross} in the stellar atmosphere with the parameters $T_{eff} = 11\,000$ K, $\lg g = 4.0$. The red dashed curve is for the LTE-model with zero-matallicity with $Y = 0.0793$. The blue dash-dotted curve is for the non-LTE-model with zero-matallicity. The black solid curve is for LTE-model with solar elemental abundances. The black dashed curve is for non-LTE-model with solar elemental abundances. The thin lines correspond to our calculations, the thick lines correspond to models calculated with TLUSTY (the models with zero-matallicity) or ATLAS9 (LTE-model with solar elemental abundances, ODF)

calculations, we consider again the model with zero-metallicity, where non-LTE effects are most important. The parameter was varied in the range from 10^{-1} to 10^{-4}. Oscillations of Λ-correction are significantly reduced with increase in δ_S, however it leads to reduce the accuracy, which can be obtained for the heat balance (i.e. iterations do not converge or converge to wrong models). The models, obtained for various δ_S, differ near the temperature minimum, which is placed higher for $\delta_S = 0.1$, in such models $T(\tau_{Ross})$ is later detached from the LTE-curve. The heat balance at depth of maximum differences between the models is by an order of magnitude better for $\delta_S = 0.01$, then for $\delta_S = 0.1$ (see Fig. III.4). If $\delta_S < 0.01$, then there are no differences neither between the models nor in the heat balance, which has been reached at the final iteration. Therefore, the optimal value of the parameter $\delta_S = 0.01$.

The temperature as a function of m in the atmosphere of the star with zero-metallicity is shown on Fig. III.2 and III.3 for various atomic models of hydrogen. The largest difference is seen between the models calculated with the hydrogen atom with $N_{max} = 10$ and $N_{max} = 30$. In case of LTE, the significant difference ($\gtrsim 100$ K) occurs only in deep layers; in non-LTE case, the such differences can be seen in upper and deep layers .

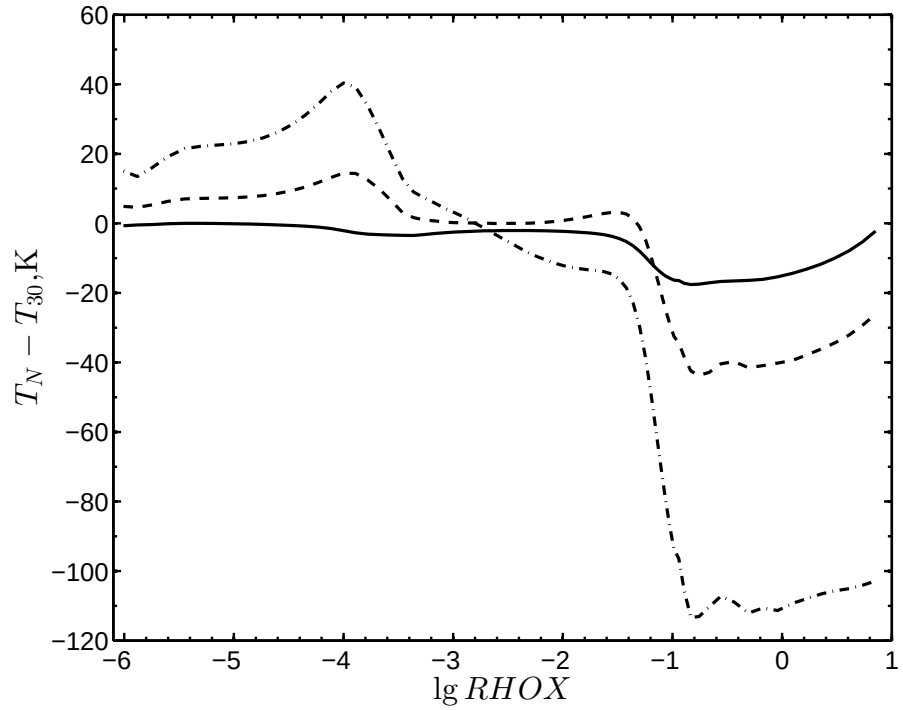

Figure III.2: The LTE-models of the star with $T_{eff} = 11\,000$ K, $\lg g = 4.0$. The temperature distribution with depth in the stellar atmosphere for various atomic models is shown relative to the atomic model with $N_{max} = 30$. The dash-dotted curve is for $N_{max} = 10$. The dashed curve is for $N_{max} = 15$. The dolid curve is for $N_{max} = 20$. The atomic data sets are E(10,15,20,30)ShE for hydrogen and N10l5 for helium. The abscissa is the mass coordinate $m \equiv RHOX$, because τ_{Ross} is slightly different for various models.

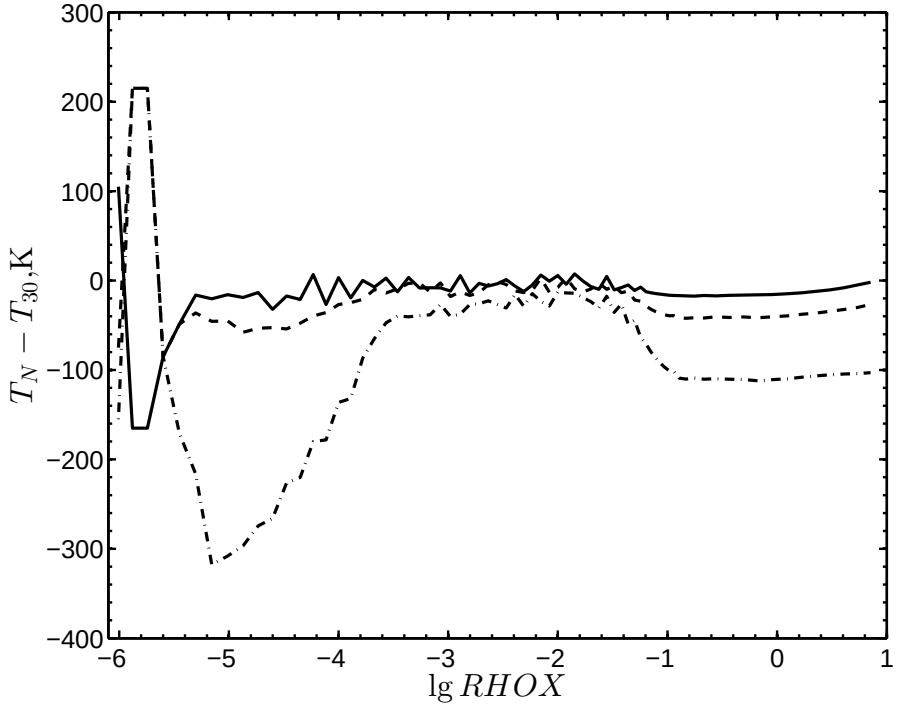

Figure III.3: The same as in Fig. III.2, but for the non-LTE-models. In the uppermost layers the difference is caused by poor convergence of the models due to inappropriate temperature corrections. In these layers the heat balance cannot be reached by means of the temperature correction schema used here.

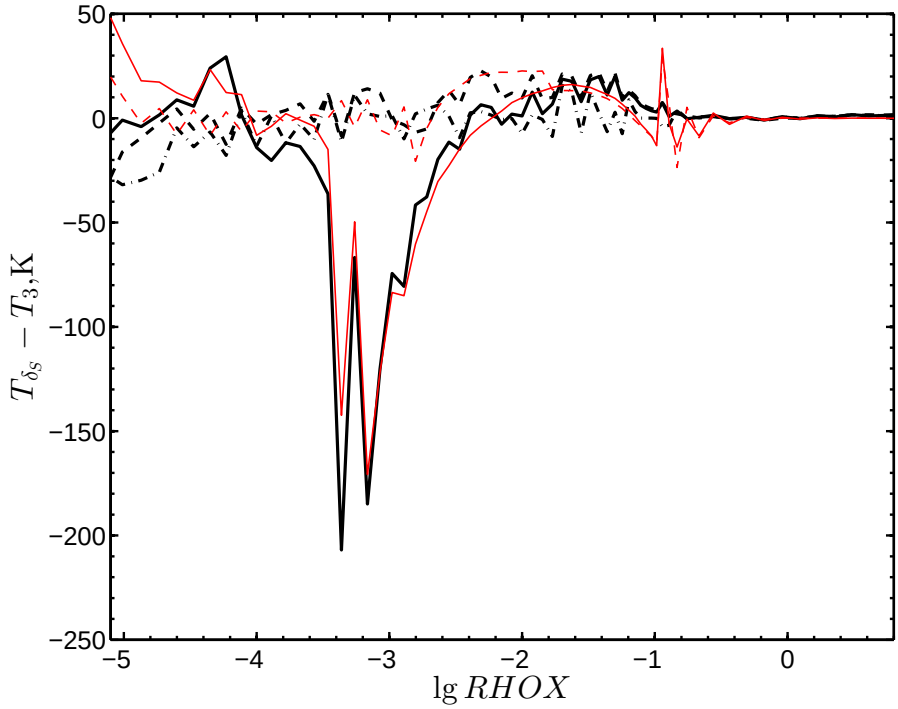

Figure III.4: The stellar atmosphere with $T_{eff} = 11\,000$ K, $\lg g = 4.0$, zero-metallicity, non-LTE. The temperature distribution with depth in the stellar atmosphere for various parameters δ_S is shown relative to the model with $\delta_S = 10^{-3}$. The solid curve is for $\delta_S = 10^{-1}$. The dashed curve is for $\delta_S = 10^{-2}$. The dash-dotted curve is for $\delta_S = 10^{-4}$. The thick curves correspond to the differences in the temperature. The thin red curves correspond to the imbalance between cooling and heating calculated as follows $2\frac{\int((1-\epsilon_\nu)\chi_\nu J_\nu - \eta_\nu)d\nu}{\int((1-\epsilon_\nu)\chi_\nu J_\nu + \eta_\nu)d\nu}$ and multiplied by "-10^7" for convenience. The uppermost layers, where the difference is caused by poor convergence of the models, are not shown.

III.2. Irradiated stellar atmospheres

Let's compare results obtained with our code and with other rezults for the case of an irradiated stellar stmosphere. The comparison is done for the model, which has been considered by Günter&Wawrzyn (2011). The parameters of the star are $T_{eff} = 4100$ K, $\lg g = 4.5$, that is close to the parameters of CTTS, which are the main purpose of the modelling. The star is irradiated by the blackbody radiation with $T_{BB} = 20000$ K. The ratio of the incident flux to the stellar flux is 5.3. The external radiation is directed perpendicular to the surface. However, strictly speaking, it is impossible in our program due to choosing of μ_i in Feautrier's method, therefore the external radiation enters the atmosphere at angles between 0^o and 27^o.

LTE and non-LTE models have been calculated for the two atomic data sets (see Fig. III.5):

The simplified model: the atomic data set for hydrogen is E20ShE, for He I is N10L5 and the 40-levels atom for He II . 30 000 frequency points between $100 - 10000$Å and 15 000 outside this range are used in OS.

The full version: the atomic data set for hydrogen is E30ShE, for He I is N10L7 and the 40-levels atom for He II . 60 000 frequency points between $100 - 10000$Å and 15 000 outside this range are used in OS.

The comparision shows that external layers of the heated atmosphere in non-LTE case are cooler than in LTE-models, and more deeper subsequent layers become hotter.

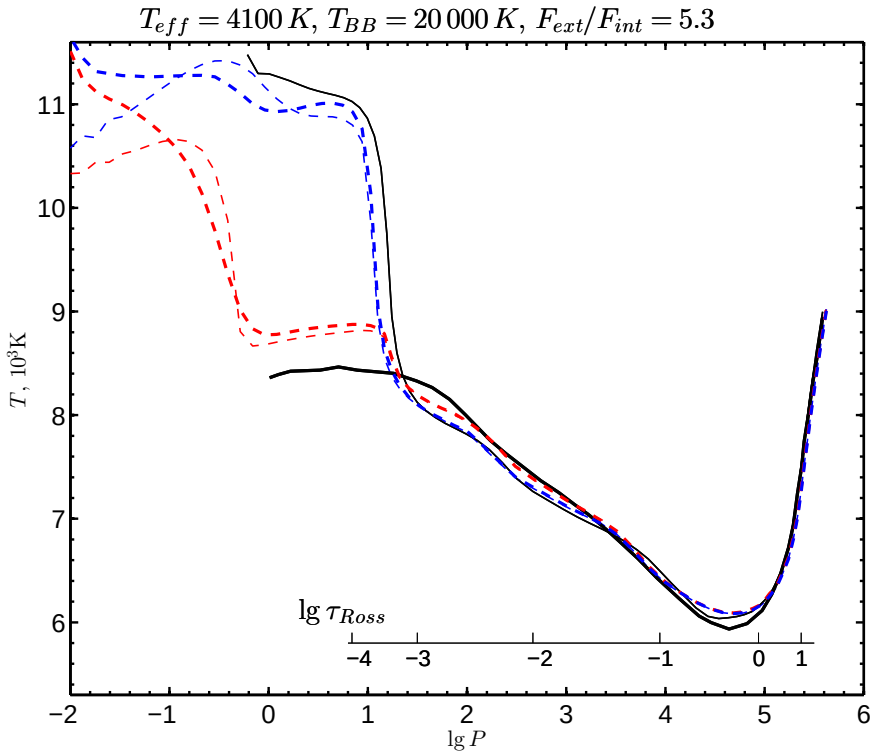

Figure III.5: Comparison with the calculations of Günter&Wawrzyn (2011) (the thick black curve). External radiation is directed perpendicular to the surface. The thin black curve is for the old LTE-model (Dodin, Lamzin, 2012). The thin blue curve is for the new LTE-model with the simplified atomic data sets and 30 000 frequency points in OS. The thick blue curve is for new LTE-model with more complicated atomic models and 60 000 frequency points in OS. The red curves are for the models with the same parameters, but calculated in non-LTE. The convection is treated in MLT, $\alpha = 2.0$. The microturbulence is $V_t = 1.0$ /. Solar elemental abundances.

Bibliography

Allen C. W., Astrophysical Quantities, 3rd Edition. London: Athlone Press. (1973)

Auer, L. H.; Mihalas, Dimitri Astrophysical Journal Supplement, vol. 24, p.193 (1972)

Berestecki V. B., Lifshits E. H., Pitaevski L. P., Quantum Electrodynamics, Nauka, Moscow (1980). in Russian

Butler K., Giddings J. Newsletter on the analysis of astronomical spectra No. 9, University of London (1985)

Castelli F., Kurucz R. L.) astro-ph/0405087 (2004)

Clark R. E. H., Abdallah J., Jr. and J. B. Mann) Astroph J., **381**, 597 (1991)

Dere K. P., Landi E., Mason H. E., Monsignori Fossi B. C., Young P. R., Astron. Astrophys. Suppl. Ser., **125**, 149 (1997)

Dimitrijevic M. S. and Sahal-Brechot S., J. Quant. Spectrosc. Radiat. Transfer **31**, 301-313 (1984)

Dodin A. V., Lamzin S. A. Astronomy Letters, **38**, 649 (2012)

Dreizler S., ASPC, 288, 69 (2003)

Fernley, J. A., Taylor K. T., Seaton M. J., J. Phys. B, 20, 6457 (1987)

Griem H. R. Astrophys. J., **132**, 883 (1960)

Golovatyj V. V., Sapar A., Feklistova T., Kholtygin A. F., Astron. Astrophys. Transactions, **12**, 85 (1997).

Günter H. M.&Wawrzyn A. C., A&A 526, 117 (2011)

Johnson L. C. Astrophysical Journal, **174**, 227 (1972)

Hauschildt P. H., Allard F., Baron E. Astrophys. J., **512**, 377 (1999)

Hubeny, I., Hummer, D.G., Lanz, T., Astron. Astrophys., **282**, 151 (1994)

Kurucz R. SAO Sp. Rep. **309** (1970)

Kurucz, R. L., , "Stellar Atmospheres: Beyond Classical Models", NATO Asi Ser., ed. L. Crivellari et al.,441 (1990)

Landi E., Del Zanna G., Young P. R. et al., Astrophys. J. Suppl. Series, **162**, 261 (2006).

Lin C. Y., Ho Y. K. Computer Physics Communications 182, 125 (2011)

Mihalas D., Stone M. E. Astrophys. J., **151**, 293 (1968)

Mihalas D. NCAR-TN/STR-76 (1972)

Mihalas D., Stellar Atmospheres. W. H. Freeman, 1978

Nahar S. N. New Astronomy **15**, 417 (2010)

Percival I. C., Richards D. Monthly Not. Roy. Astron. Soc. **183**, 329 (1978)
Przybilla N., Butler K., ApJ, **609**, 1181 (2004)
Przybilla N., A&A, 443, 293 (2005)
van Regemorter H. Astrophys. J., **136**, 906 (1962)
Seaton, M.J., 1962. in "Atomic and Molecular Processe", New York Academic Press
Stehle C., Hutcheon R. Astron. Astrophys. SuppL. Ser. 140, 93 (1999)